ORGANOMETALLICS

pubs.acs.org/Organometallics Article

Breaking and Entering: Diazene Cleavage and Insertion into U(III)−Si Bonds

Nathan J. Lin, Kelly L. Gullett, Ushindi K. Muna, Ryan Galloway, Matthias Zeller, and Suzanne C. Bart*

Cite This: *Organometallics* 2025, 44, 289−299 Read Online

ACCESS | Metrics & More | Article Recommendations | Supporting Information

ABSTRACT: Treatment of trivalent [K(18-crown-6)][U(I)$_2${(Si(SiMe$_3$)$_2$SiMe$_2$)$_2$O}] (**1-crown**) with aryl diazenes generated a series of uranium(IV) species of the form [(THF)U(I)$_2${N(R/R′)Si(SiMe$_3$)$_2$SiMe$_2$}$_2$O] (R = R′ = Ph (**2-Ph**), 4-FC$_6$H$_4$ (**2-F**), 4-MeC$_6$H$_4$ (**2-Tol**), 4-OMeC$_6$H$_4$ (**2-Mes**), and R = 4-MeC$_6$H$_4$, R′ = Ph (**2-TolPh**). Activation of an ortho-substituted diazene, (2,4,6-Me$_3$C$_6$H$_2$N)$_2$ (MesN═NMes), forms **2-Mes**, [K(18-crown-6)][U(I)$_3${N(Mes)Si(SiMe$_3$)$_2$SiMe$_2$}$_2$O] (**2-MesKI**), and ([K(18-crown-6][U(I)(NMes)(N[Mes]-3,3,5,5-Me$_4$2,2,6,6-(SiMe$_3$)$_4$-tetrasil-3-oxane)]) (**3-Mes**). The increased sterics of this *ortho*-substituted substrate slowed insertion, facilitating the observation of **3-Mes** by in situ NMR spectroscopy. The redox potentials of the aryl diazenes (R−N═N−R′) were studied using cyclic voltammetry to elucidate their electronic contributions toward their reactivity with **1-crown**. The reaction of **1-crown** and (*Z*)-11,12-dihydrodibenzo[*c*,*g*][1,2]diazocine is also described, forming the [(THF)U(I)$_2${[N(C$_7$H$_6$)]$_2$Si(SiMe$_3$)$_2$SiMe$_2$}$_2$O] (**2-diazonine**) and {(THF)$_2$U(I)$_2$[N(C$_7$H$_6$)]$_2$}$_2$ (**4**) dimers.

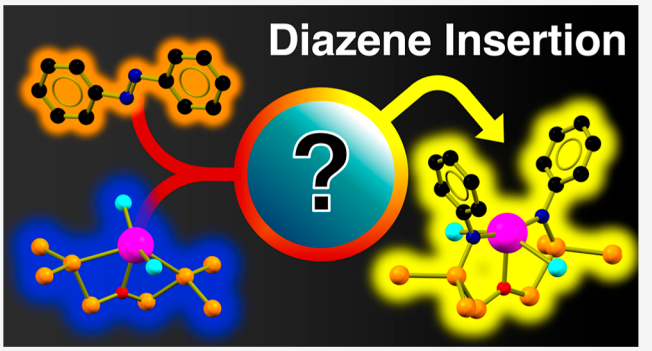

INTRODUCTION

Insertion of small molecules into M−Si bonds is a fundamental transformation in organometallic chemistry that is used to generate silyl-based building blocks for the synthesis of fine chemicals.[1] Transition metal−silyl bonds are often invoked as intermediates in silylation reactions, and these have been extensively studied.[2−5] For instance, the modified Chalk−Harrod hydrosilylation mechanism proposes an alkene insertion into a M−Si bond.[3] Clearly defining the sequence of which insertion happens with silylation reactions is important for developing and designing organometallic transformations.[2]

The insertion of unsaturated nitrogen-based substrates into M−Si bonds is rarer than its carbon-based counterparts.[6,7] One example by Moreau and co-workers is the insertion of nitriles into a chelating silyl iron complex that results in reductive elimination of *N*,*N*-bis(silyl)enamines.[8] Tilley and co-workers have reported the insertion of N$_2$CPh$_2$ into a Ta(V)−Si bond, resulting in an η^2-side-on complex.[9] M−Si cleavage by amines regenerates Lewis pair interactions and formation of silane salts through the formation of [Me$_3$SiNMe$_3$]$^+$[Co(CO)$_4$]$^-$ from Me$_3$Si−Co(CO)$_4$ and NH$_3$, as demonstrated by Bald and MacDiarmid.[7] Nikonov and co-workers describe organometallic complexes featuring both imide and silyl ligands that undergo reversible silylamide transformations with metal hydrides.[10−12]

In comparison to transition metals, silyl chemistry in the actinide series has only been reported for a few examples of An−Si bonds. Kaltsoyannis, Liddle, Mills, and co-workers have synthesized and characterized isostructural thorium and uranium silanide complexes, An(Cp′)$_3$(Si(SiMe$_3$)$_3$) (An = Th, U; Cp′ = η^5-C$_5$H$_4$SiMe$_3$).[13,14] Similarly, An(Cp′)$_2$(Si(SiMe$_3$)$_3$Cl) has also been characterized by some members of that team.[15]

The lack of insertion chemistry into An−Si bonds can be attributed to multiple factors: (1) actinide species featuring An−Si bonds are difficult to isolate, (2) these bonds are generally sensitive to decomposition,[16,17] or (3) the insertion products are not always well characterized.[18] For instance, Cummins and co-workers found that the bulky—Si(SiMe$_3$)$_3$ group was necessary to stabilize the U−Si bond in (Me$_2$C$_6$H$_3$[^{t}Bu]N)$_3$U(IV)Si(SiMe$_3$)$_3$, but this species was resistant to the insertion of carbon monoxide, isocyanates, and cyanides into U−Si bonds. Using an isocyanide, ^{i}PrNC, afforded an intractable mixture of products.[19] In another example, Porchia and co-workers reported the insertion of 2,6-Me$_2$C$_6$H$_3$NC into Cp$_3$U(IV)−SiPh$_3$ that generated a U(IV) ion bound to η^2−[2,6-Me$_2$C$_6$H$_3$N═CSiPh$_3$].[20] To our

Received: October 22, 2024
Revised: November 20, 2024
Accepted: November 25, 2024
Published: December 20, 2024

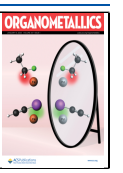

https://doi.org/10.1021/acs.organomet.4c00449
Organometallics 2025, 44, 289−299

knowledge, formal U(III)−Si insertion reactions have not been reported, though uranium(III) silylenes have been shown to be displaced by carbon monoxide, likely due to its superior donicity.[21]

Recently, we have reported the synthesis and characterization of a rare, trivalent silyluranium species, [K(18-crown-6)]-[$U(I)_2\{(Si(SiMe_3)_2SiMe_2)_2O\}$] (**1-crown**)[22], that uses a chelating silyl system developed by Baumgartner and Marschner.[23,24] The strong reducing power of U(III) in conjunction with reactive U−Si bonds in this system presented a possibility for the activation of thermodynamically strong N═N bonds, such as those in diazenes. The geometry of the silyl ligand allows access to uranium by the displacement of the coordinated solvent. Herein, we report reactivity studies with aryl diazenes that vary in their electronic properties. These studies are supported by cyclic voltammetry, which has helped to elucidate the dependence of substituents on the diazene reduction potential. An intermediate stabilized by *ortho*-substitution of the diazene is also observed, providing mechanistic insights of the title reaction.

RESULTS AND DISCUSSION

To investigate the activation of diazenes by a uranium(III)-silyl species, 1 equiv. of azobenzene was introduced to a blue THF solution of **1-crown** at −35 °C (Scheme 1). During workup, a

Scheme 1. Synthesis of Family 2 from 1-Crown

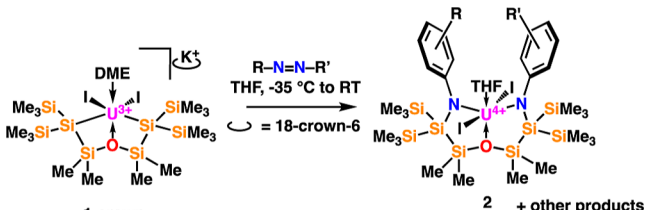

		Yield
2-F:	R = R' = 4-F	22%
2-Ph:	R = R' = Ph	28%
2-PhTol:	R = Ph, R' = 4-MePh	43%
2-Tol:	R = R' = 4-MePh	27%
2-OMe:	R = R' = 4-OMePh	43%
2-Mes:	R = R' = 2,4,6-Me_3Ph	26%

yellow, pentane-soluble product and an orange, pentane-insoluble species were isolated. The yellow product was stable and lent itself to full characterization, whereas the orange product decomposed over hours (see below).

To identify the yellow product, single crystals of the azobenzene derivative suitable for X-ray diffraction were grown from a concentrated pentane solution at −35 °C. Collection and refinement of the diffraction data revealed N═N cleavage of azobenzene, along with the insertion of a phenylimido group into the U−Si bonds, forming [$(THF)U(I)_2\{N(Ph)Si(SiMe_3)_2SiMe_2\}_2O$] (**2-Ph**) (Figure 2 and Table 1). The uranium ion of **2-Ph** is a distorted octahedron with U−N distances of 2.213(4)−2.217(4) Å.[25] These distances are ca. 0.07 Å shorter than in the homoleptic tetrahedral silylamide, tetrakis(bis(trimethylsilyl)amido)uranium(IV), $U(N(SiMe_3)_2)_4$, that has U−N distances of 2.2941(17)−2.3013(17) Å.[25] The N−U−N angle of **2-Ph** is near-linear (173.69(13)°; all N−U−N angles are defined as opening toward the siloxide unit). The U−O distances are 2.493(3) and 2.445(3) Å for siloxane and THF, respectively, and are shorter when compared to the *cis* U−O distances of 2.586 and 2.602 Å in bis(bis(trimethylsilyl)amido)dichlorouranium(IV)-(dimethoxyethane), $U(Cl)_2(N(SiMe_3)_2)_2$.[26] The U−I bond

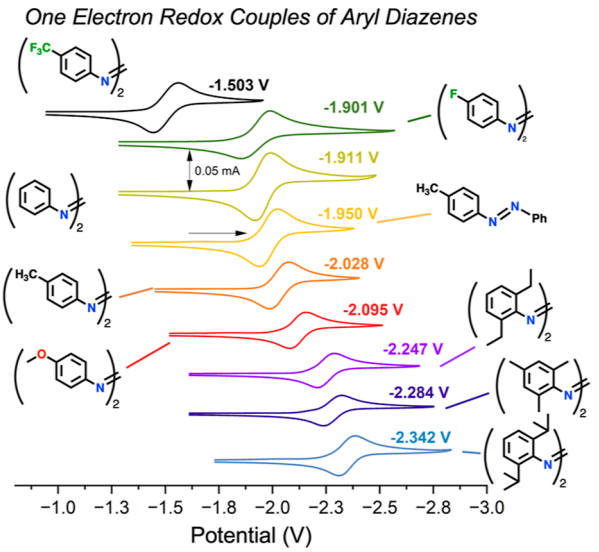

Figure 1. Cyclic voltammograms of one electron redox couples of 3 mM diazenes in 0.1 M NBu_4PF_6 in THF (V vs internal $Fc^{+/0}$). Estimated standard deviation is ±0.005 V.

distances of 3.0432(4) and 3.0850(4) Å and the I−U−I angle of 177.737(11)° are typical for U(IV) complexes,[27,28] . The activation of azobenzene by **1-crown** is a rare example of an organouraniumsilyl complex cleaving a N−N multiple bond.[1,6] The formation of **2-Ph** through the insertion of cleaved azobenzene into **1-crown** is the first crystallographically characterized insertion complex for U−Si chemistry.

Liddle, Mills, and co-workers report a recent example of a Y(III) silanide that undergoes carbodiimide insertion without further oxidation,[29] as the Y(III), d^0 ion is incapable. Analogous chemistry was noted with azobenzene, which is in contrast with the observed chemistry here. Trivalent **1-crown** is able to undergo oxidation to U(IV), and this difference in accessible oxidation state, paired with U(III)'s reducing ability, facilitates complete N−N cleavage of azobenzene.

In order to expand this reaction to more diazenes, the reduction potentials of diazenes with varying steric and electronic properties were studied electrochemically. The half-wave potentials ($E_{1/2}$) for aryl diazenes were electrochemically elucidated in THF (0.1 M $TBAPF_6$) and were found to exhibit a Nernstian behavior (Figure 1). As expected, the fluorinated diazenes $(4\text{-}CF_3C_6H_4N)_2$ and $(4\text{-}FC_6H_4N)_2$ have the mildest reduction potentials of the series, −1.503 V and −1.901 V vs $Fc^{+/0}$ (±5 mV), respectively. Electron donating diazenes $(4\text{-}OMeC_6H_4N)_2$, $(2,6\text{-}Et_2C_6H_3N)_2$, MesN═NMes, and $(2,6\text{-}^iPr_2C_6H_3N)_2$ reduce at more negative potentials, −2.095, −2.247, −2.284 and −2.342 V, respectively, due to their electron-rich nature. The $E_{1/2}$ value for $(4\text{-}MeC_6H_4N)_2$ is slightly more negative than for mixed $4\text{-}MeC_6H_4N$═NPh due to the inclusion of an additional methyl substituent.

This series of 4-substituted diazenes were then used to synthesize, in an analogous procedure to **2-Ph**, additional family members of the form, [$(THF)U(I)_2\{N(R/R')Si(SiMe_3)_2SiMe_2\}_2O$] (R = R′ = 4-F-$C_6H_4$ (**2-F**), 4-Me-C_6H_4 (**2-Tol**), 4-OMe-C_6H_4 (**2-OMe**), 2,4,6-$Me_3C_6H_2$ (**2-Mes**), and R = 4-MeC_6H_4, R′ = Ph (**2-TolPh**)) (Scheme 1). Interestingly, **1-crown** does not react cleanly with $(4\text{-}CF_3C_6H_4N)_2$, resulting in intractable products. Treating **1-crown** with $(2,6\text{-}Et_2C_6H_3N)_2$ did not cause a reaction at room temperature,

https://doi.org/10.1021/acs.organomet.4c00449
Organometallics 2025, 44, 289−299

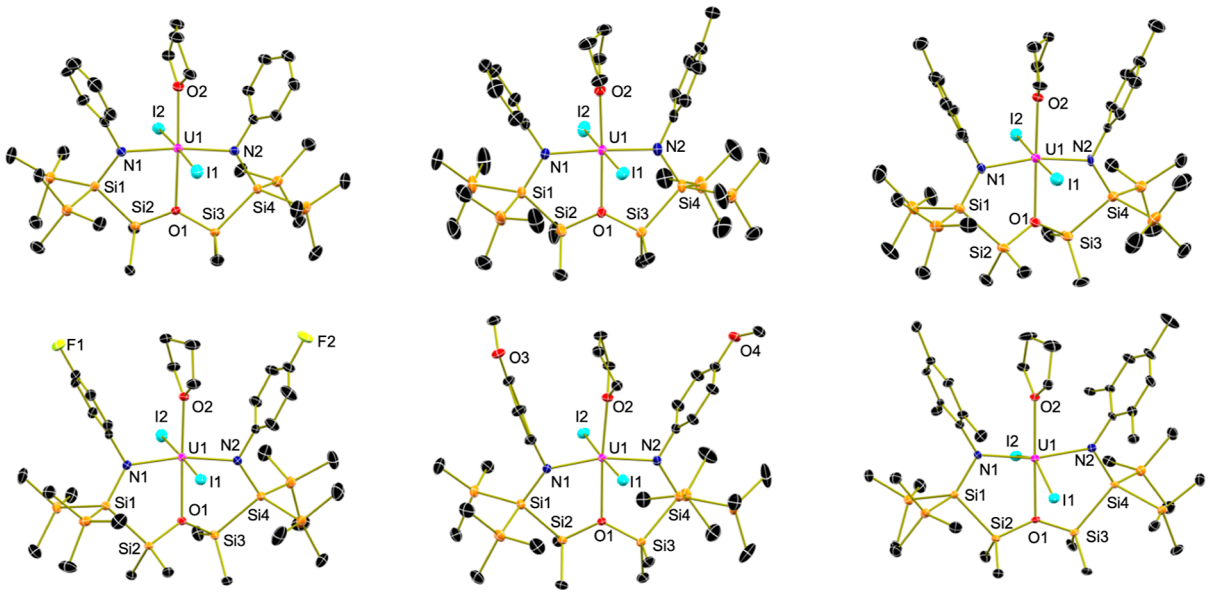

Figure 2. Molecular structures (from left to right, top to bottom) of **2-Ph**, **2-TolPh**, **2-Tol**, **2-F**, **2-OMe**, and **2-Mes** shown with 30% probability ellipsoids. Hydrogen atoms, outer-sphere solvent molecules, and disordered moieties have been removed for clarity.

Table 1. Metrical Parameters for 2-Ph, 2-TolPh, 2-Tol, 2-F, 2-OMe, 2-Mes, 2-MesKI, 2-Diazonine, 3-Mes, and 4

	U–N (Å)	N–U–N (°)[a]	U–O_{Si} (Å)	U–O_{THF}(Å)	U–I(Å)	I–U–I (°)[a]
2-F	2.2064(16)	168.47(6)	2.5395(13)	2.4349(14)	3.0529(2)	178.519(6)
	2.2135(16)				3.0875(2)	
2-Ph	2.213(4)	173.69(13)	2.493(3)	2.445(3)	3.0850(4)	177.737(11)
	2.217(4)				3.0432(4)	
2-TolPh	2.214(3)	174.90(11)	2.483(2)	2.417(2)	3.0531(8)	177.344(10)
	2.216(3)				3.0682(8)	
2-Tol	2.209(7)	167.3(3)	2.550(6)	2.439(6)	3.0474(8)	177.98(2)
	2.212(7)				3.0776(8)	
2-OMe	2.200(2)	164.35(8)	2.5695(16)	2.471(9)	3.0548(2)	177.723(6)
	2.202(2)				3.1009(2)	
2-Mes	2.240(7)	194.3(2)	2.458(5)	2.434(5)	3.0778(8)	152.81(2)
	2.247(7)				3.0959(8)	
2-MesKI	2.248(6)	191.0(3)	2.488(8)		3.0667(11), 3.0743(10), 3.0396(9)	109.36(3), 100.07(3), 150.582(3)
2-diazonine	2.199(4) to	211.72(14)	2.321(3)		3.0316(4) to 3.0539(4)	166.553(10)
3-Mes	2.212(3)	212.64(14)	2.346(3)		3.0530(2)	166.497(11)
4	1.879(6) to 1.880(5)	179.3(3)		2.422(5)	3.0767(7) to 3.1920(5)	142.138(9), 142.347(9), 75.308(17)

[a]Angles are reported as opening toward the siloxane unit of the silylamide ligand.

and heating the reaction vessel to 45 °C gave an intractable mixture. An analogous reaction with $(2,6\text{-}^{i}Pr_2C_6H_3N)_2$ also proved challenging as even elevated temperatures did not produce a reaction. These observations track with the more negative reduction potentials of these species, along with their increased *ortho*-steric demands.

Compounds **2-Ph**, **2-F**, **2-TolPh**, **2-Tol**, and **2-OMe** were characterized by ^{1}H NMR spectroscopy (C_6D_6, ambient temperature). All compounds showed resonances spanning −90 to 75 ppm and are consistent with C_{2v} symmetry in solution (with the exception of **2-TolPh**, which has C_s symmetry, as the NMR shifts appear in pairs due to inequivalent substituents). The ^{1}H $SiMe_3$ resonances range from 15.45 to 16.81 ppm, whereas the resonances for the $SiMe_2$ groups are visible from −25.96 to −28.60 ppm. The resonances for the *meta*-protons of the aryl rings are between 24.43 and 29.12 ppm, while the *ortho*-protons, where applicable, appear from 68.70 to 78.47 ppm.

^{29}Si NMR spectroscopy was useful in the characterization of these species, and representative data were collected. For **2-OMe**, the $^{29}Si\{^{1}H\}$ NMR spectrum showed three resonances: two downfield-shifted resonances at 172.0 and 142.9 ppm and another upfield resonance at −91.2 ppm (Figure S4). The resonance of the nitrogen-bound silicon atom could be assigned due to its absence at 142.9 ppm in the ^{29}Si INEPT (Insensitive Nuclei Enhanced by Polarization Transfer) spectrum, which lacks short-range coupling to protons of the $SiMe_3$ (−91.2 ppm) and $SiMe_2$ (172.0 ppm) linkers. Similar resonances could be observed in the ^{29}Si INEPT spectrum for **2-TolPh** at δSi =165.9, 160.3, −96.8, and −102.7 ppm (Figure S7). Despite multiple attempts, the ^{29}Si NMR spectra of **2-F**, **2-Ph**, **2-Tol**, and **2-Mes** did not show ^{29}Si signals, likely due to paramagnetic broadening.

https://doi.org/10.1021/acs.organomet.4c00449
Organometallics 2025, 44, 289−299

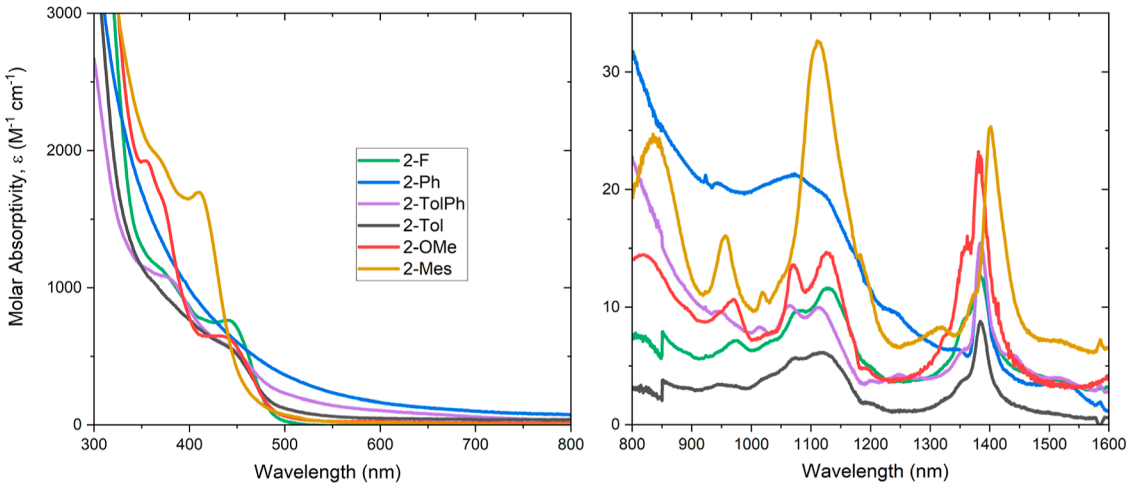

Figure 3. Electronic absorption spectroscopic data collected in the UV−visible (left) and NIR regions (right) (THF, ambient temperature) for **2-F**, **2-Ph**, **2-TolPh**, **2-Tol**, **2-OMe**, and **2-Mes**. The change in intensity at 850 nm is due to a detector switch.

Compared to trivalent **1-crown**, the NMR signals of **2-OMe** and **2-TolPh** are shifted downfield, typical for U(IV) complexes (0 to −150 ppm),[30] indicative of oxidation and consistent with lower electron density around a U(IV) ion.[30] P. Arnold and co-workers reported strong downfield ^{29}Si shifts at 160 and 152 ppm assigned to the siloxide ligands of calixpyrrole U(V) macrocycles.[31] The similarity in ^{29}Si shift of **2-OMe** and **2-TolPh** compared to the U(V) siloxide is likely due to the two-bond distance from the paramagnetic uranium center. For comparison, the free ligand $\{K(Si(SiMe_3)_2SiMe_2)\}_2O$ resonates at 27.6, −7.0, and −185.7 ppm.[23] In comparison with other uranium−silicon complexes, the U-bonded Si atom of Réant and co-workers' tris-Cp′U(IV)−$Si(SiMe_3)_3$ resonates at −137.09 ppm.[13] This stark difference in ^{29}Si NMR shift between silanide and silylamide represents a drastic change in silanide character once the N atom intercepts the U−Si bond and thus becomes less reactive.

Electronic absorption spectroscopic data of **2-Ph**, **2-F**, **2-TolPh**, **2-Tol**, and **2-OMe** were recorded to elucidate their electronic structures (Figure 3). The UV−visible regions of the spectra contain large color-producing bands from 350 to 450 nm (ε = 2000 to 780 M^{-1} cm^{-1}) for these yellow compounds (Figure 3).[32] The near-infrared region shows two sets of absorbance bands for **2-Ph**, **2-F**, **2-TolPh**, **2-Tol**, and **2-OMe**: one set from 950 to 1190 nm (ε = 10 to 30 M^{-1} cm^{-1}) and another set from 1360 to 1400 nm (ε = 15 to 25 M^{-1} cm^{-1}). These two sets of bands in the near-infrared region are consistent with weak Laporte-forbidden 5*f*−5*f* transitions, indicating a U(IV) oxidation state. These are significantly different than for the more intense and broader 5*f*−5*f* transitions noted for trivalent **1-crown**.[22]

As for **2-Ph**, X-ray crystallographic data were collected on single crystals of **2-TolPh**, **2-Tol**, **2-F**, **2-OMe**, and **2-Mes** grown from slow evaporation of either pentane or hexane at −35 °C (Figure 2, Table 1, crystallization details in the Supporting Information). Refinement showed that these species are isostructural, with the U−N (2.200(2) to 2.217(4) Å) and U−I (3.0432(4) to 3.1009(2) Å) distances correlating to other U(IV) species.[25,33] For comparison, typical trivalent U−N and U−I distances are more than 2.3 and 3.1 Å, respectively.[22,34,35] The geometric parameters of **2-TolPh** are comparable to those of **2-Ph** and **2-Tol**, but they are unreliable due to methyl/hydrogen disorder of the aryl substituents in the crystal structure.

The U−N bond lengths for **2-Ph**, **2-TolPh**, and **2-Tol** are the same within error (2.209(7)−2.217(4) Å); the electron-donating *para*-methoxy group (**2-OMe**: 2.200(2)−2.202(2) Å) does not show a significant deviation from these values. A correlation is noted with the U−O_{Si} distance, where electron-donating aryl groups have slightly increased U−O_{Si} distances compared to their electron-withdrawing counterparts (**2-F**: 2.5395(13), **2-Tol**: 2.550(6), and **2-OMe**: 2.5695(16) Å). In addition, the electron donor strength of the aryl substituent causes a decrease in the N−U−N angle (**2-F**: 168.47(6), **2-Tol**: 167.3(3), and **2-OMe**: 164.35(8)°). Based on the U−O_{Si} distances and N−U−N angles, electron-withdrawing aryl substituents cause uranium to approach the silyl ether more closely to gain electron density.

The FTIR spectra of **2-F**, **2-Ph**, **2-TolPh**, **2-Tol**, **2-OMe**, and **2-Mes** show U−N absorption from 962 to 965 and 835 to 838 cm^{-1}. These stretches are similar to the U−N−Si asymmetric (990 cm^{-1}) and symmetric stretches (812 cm^{-1}) reported by Andersen for $U(III)(N(SiMe_3)_2)_3$[36] and Mills for $U(III)(N(SiMe_2{}^tBu)_2)_3$.[37] Other reports of silylamide uranium complexes have absorptions in this region as well.[38] Based on these infrared data, the substituents do not have a significant effect on the U−N bond strength.

Compound **2-Mes** was analyzed using X-ray crystallography to elucidate the structural effects of the *ortho*-steric bulk (Figure 2 and Table 1). This species is isostructural with the rest of the compound **2** family, with a distorted octahedral uranium ion. The U−N distances of **2-Mes** (2.240(7)−2.247(7) Å) are substantially longer than that of the *ortho*-unsubstituted **2-F**, **2-Ph**, **2-TolPh**, **2-Tol**, and **2-OMe** complexes, indicating heavy influence by *ortho*-sterics. The uranium ion of **2-Mes** is closer to the O_{Si} atom (**2-Mes**: U−O_{Si} = 2.458(5) Å) than **2-Ph**. The N−U−N bite angle of the ligand (**2-Mes**: N−U−N = 194.3(2)°) is large relative to the siloxane unit, showing the electronic trend established with **2-Ph**, **2-Tol**, and **2-OMe** (N−U−N is acute relative to the siloxane unit) does not hold and is distorted by *ortho*-sterics. Similarly, it is evident that the *ortho*-methyl groups affect the angle of the iodide ligands, decreasing the I−U−I angle (**2-Mes**: 152.81(2)°) from the near-linear I−U−I angles found in

https://doi.org/10.1021/acs.organomet.4c00449
Organometallics 2025, 44, 289−299

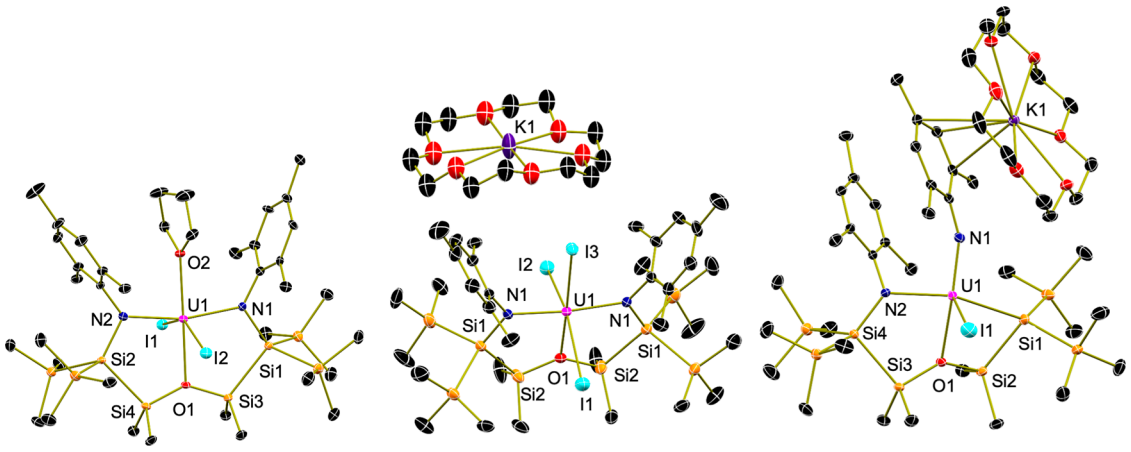

Figure 4. Molecular structures of **2-Mes** (left), **2-MesKI** (center), and the *S* enantiomer of **3-Mes** (right) shown with 30% probability ellipsoids. Hydrogen atoms and disordered moieties have been removed for clarity.

2-F (178.519(6)°), **2-Ph** (177.737(11)°), **2-Tol** (177.98(2)°), and **2-OMe** (177.723(6)°).

In order to gain a mechanistic understanding of the observed insertion chemistry, a ligand crossover experiment was performed by treating **1-crown** with a 1:1 mixture of (Ph-N)$_2$/(4-Me-C$_6$H$_4$N)$_2$. Analysis of the reaction mixture by ^{1}H NMR spectroscopy (Figure S16) showed the formation of both **2-Tol** and **2-Ph**. No **2-TolPh** was observed, supporting the idea that ligand crossover *does not* occur during the course of the reaction. The absence of ligand crossover indicates that no free [NR]$^{2-}$ units are liberated or scrambled across two uranium centers.

As initially discussed, during the formation of **2-Ph**, **2-F**, **2-TolPh**, **2-Tol**, and **2-OMe**, an orange product was also generated. This species decomposed rapidly, eluding full characterization. We hypothesized that the decreased reaction rate for the insertion of the mesityl derivative in forming **2-Mes** might facilitate the characterization of this orange side product. Analysis by ^{1}H NMR spectroscopy showed resonances spanning from −155 to 55 ppm, the number and integration values supporting asymmetry in solution (Figures S23 and S27).

Fortunately, red single crystals of this side product derived from the **2-Mes** synthesis suitable for X-ray diffraction could be obtained from layering pentane onto a concentrated Et$_2$O solution (Figure 4 and Table 1). Collection and refinement of the crystallographic data revealed the formation of [K(18-crown-6][UI(NMes)(N[Mes]-3,3,5,5-Me$_4$-2,2,6,6-(SiMe$_3$)$_4$-tetrasil-3-oxane)] (**3-Mes**). Compound **3-Mes** features a pentacoordinate distorted square pyramidal (τ^5 = 0.419) uranium ion with the trichelating silylamide ligand (U1−N2 = 2.2901(15) Å; U1−Si1 = 3.0658(5) Å), a THF molecule (U1−O1 = 2.6167(12) Å), an imido (U1−N1 = 1.9810(15) Å), and an iodide ligand (U1−I1 = 3.0530(2) Å), all of which are charge-balanced by a crowned potassium countercation. The *R* and *S* enantiomers of **3-Mes** cocrystallized in the unit cell (Figure S61).

The electronic structure of **3-Mes** was interrogated using electronic absorption spectroscopy in the UV−visible and NIR regions and compared to that of **2-Mes** (Figure S44). Multiple weak *f*−*f* transitions in the NIR region at 1040 (ε = 17 M^{-1} cm^{-1}), 1095 (ε = 15 M^{-1} cm^{-1}), and 1195 nm (ε = 20 M^{-1} cm^{-1}) correlate to U(IV) ion. The broad band in the UV−visible region at 575 nm (ε = 200 M^{-1} cm^{-1}) is likely responsible for the red−orange color of **3-Mes**, which contrasts with that of yellow **2-Mes**.

Mechanistic insight into the formation of **3-Mes** was gained by treating a THF-d_8 solution of **1-crown** with 1 equiv of MesN = NMes (Scheme 2, Figure S29, center). Analysis by ^{1}H

Scheme 2. THF Synthesis of 2-Mes and 3-Mes

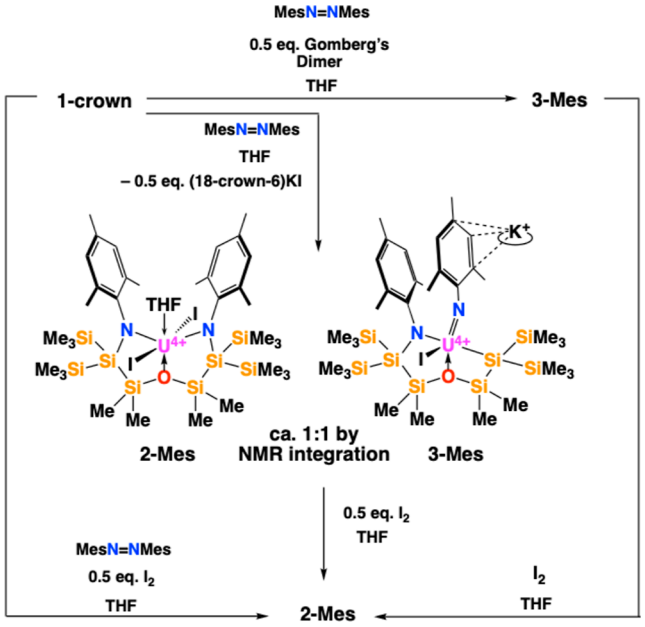

NMR spectroscopy showed resonances in a 1:1 ratio for both **2-Mes** and **3-Mes** after the consumption of reagents (Figure S31 and Scheme 2). Upon workup, **2-Mes** and **3-Mes** were isolated in 31% and 25%, respectively, along with (18-crown-6)KI. The concurrent formation of these products supports that I$^\bullet$ is formed through U−I homolysis and is likely a source for side reactions. It is proposed that 2 equiv of homolyzed I$^\bullet$ recombines with **3-Mes** to form **2-Mes** and (18-crown-6)KI.

With this hypothesis, an experiment was performed to determine if the recombination of homolyzed I$^\bullet$ during the formation of **3-Mes** (Scheme 2, top) could be prevented. A cold mixture of MesN═NMes and 0.5 equiv of Gomberg's dimer (Ph$_2$C═C$_6$H$_5$−CPh$_3$) was added to a cold THF solution of **1-crown**. Upon warming to ambient temperature

https://doi.org/10.1021/acs.organomet.4c00449
Organometallics 2025, 44, 289−299

over the course of 3 h, the solution turned dark red/orange, and the ^{1}H NMR spectrum of the crude mixture indicated clean formation of **3-Mes**, without the presence of **2-Mes** (Figure S29, bottom). In this case, the trityl radical traps I$^\bullet$ (formed from U−I homolysis), preventing in situ reactivity of 2 equiv of I$^\bullet$ and **3-Mes** and preventing the formation of **2-Mes**.

The doubly inserted **2-Mes** can be generated independently from **3-Mes** by increasing the I$^\bullet$ concentration. For example, addition of 0.5 equiv of I_2 to a mixture of **2-Mes** and **3-Mes** in THF-d_8 resulted in full conversion to **2-Mes** (Scheme 2, bottom). Alternately, addition of 1 equiv of I_2 to a THF solution of **3-Mes** formed **2-Mes** (Scheme 2, right). Because the addition of I_2 is equal to the addition of 2 equiv I$^\bullet$, when introduced to **3-Mes**, silyl migration to the imido N-atom and addition to the uranium occur, along with oxidation to U(IV). Direct one-pot synthesis of **2-Mes** can be achieved by the simultaneous addition of MesN═NMes and 0.5 equiv I_2 to **1-crown** (Scheme 2, left).

Divergent reactivity is observed in nondonating solvents, however. When an equimolar mixture of **2-Mes** and **3-Mes** was treated with 0.5 equiv I_2 (C_6D_6), [K(18-crown-6)][U(I)$_3${N-(Mes)Si(SiMe$_3$)$_2$SiMe$_2$}$_2$O] (**2-MesKI**) precipitated from pentane (Scheme 3). This material was confirmed by X-ray

Scheme 3. Convergent Synthesis of Pure 2-Mes from a Mixture of 2-Mes and 3-Mes in C_6D_6

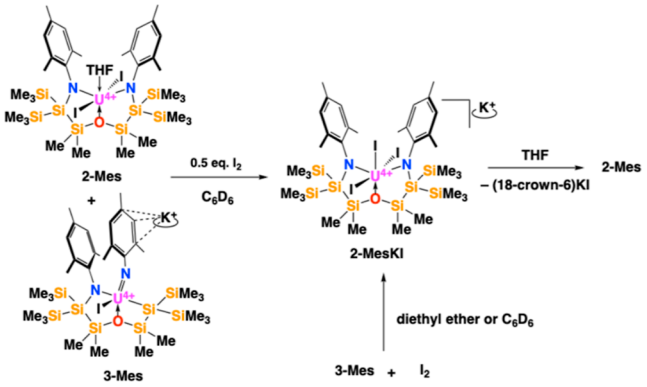

crystallography (Figure 4 (center) and Table 1). Compound **2-MesKI** contains a six-coordinate uranium ion with a chelating silyl ligand, three meridional iodide ligands, and an outer sphere potassium cation, which make this species equivalent to a KI adduct of **2-Mes**. In support, when **2-MesKI** is stirred in THF, (18-crown-6)KI is eliminated forming **2-Mes**. The equatorial iodide in **2-MesKI** has a U−I distance of 3.0396(9) Å and is ca. 0.03 Å shorter than its axial counterparts (3.0668(11) to 3.0743(10) Å). Furthermore, the sequestered potassium countercation does not coordinate to an iodide ligand, which is in contrast to the solid-state structure of **1-crown**.[22] Compound **2-MesKI** was also generated by the addition of 1 equiv I_2 to **3-Mes** in Et_2O or C_6D_6, which contrasts the previously mentioned result in THF.

To explore the scope of the NR insertion into U−Si bonds, geometric inhibition was attempted by the addition of 1 equiv of (*Z*)-11,12-dihydrodibenzo[*c*,*g*][1,2]diazocine and 0.5 equiv of I_2 to **1-crown**. Single crystals obtained from this reaction mixture from concentrated pentane showed insertion of this substrate into both U−Si bonds (Figure 5 (top), Table 1), forming [(THF)U(I)$_2${[N(C$_7$H$_6$)]$_2$Si(SiMe$_3$)$_2$SiMe$_2$}$_2$O] (**2-diazonine**) by X-ray crystallographic analysis. This demonstrated that despite the chelation of the aryl-linked ligand, insertion still occurred readily. The U−N distances of **2-diazonine** (2.199(4) to 2.212(3) Å) are similar to those found in **2-Ph**, **2-TolPh**, **2-Tol**, **2-F**, **2-OMe**, and **2-Mes**. Based on the molecular structure, the anilido aryl rings are coplanar with the silylamide ligand backbone, where the ethane-1,2-diyl linker prevents THF coordination. This is in contrast to **2-Ph**, **2-TolPh**, **2-Tol**, **2-F**, **2-OMe**, and **2-Mes**, where the aryl rings are perpendicular to the silylamide ligand backbone, allowing space for the coordinating solvent. Additionally, blockage of the sixth coordination site of **2-diazonine** by the chelator prevents THF coordination.

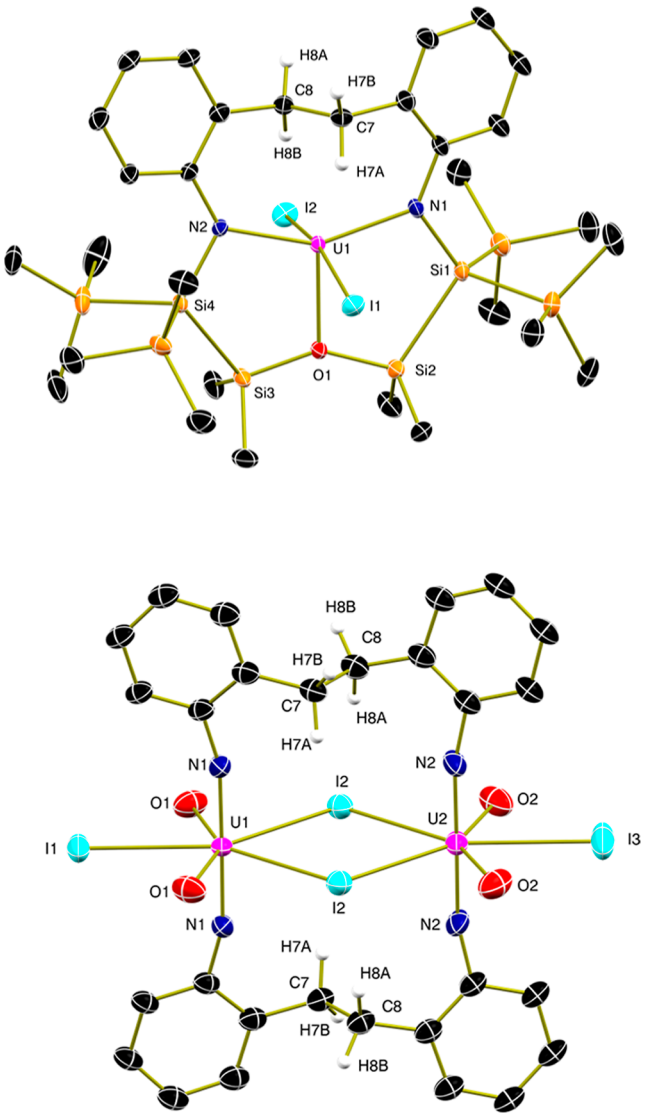

Figure 5. Molecular structure of **2-diazonine** (top) and **4** (bottom) shown with 30% probability ellipsoids. Aromatic and methyl hydrogen atoms, THF carbon atoms, and disordered moieties have been removed for clarity.

During the analysis of **2-diazonine**, another product was observed by X-ray crystallography, a U(VI) bis(imido) dimer {(THF)$_2$U(I)$_2$[N(C$_7$H$_6$)]$_2$}$_2$ (**4**) (Figure 5 and Table 1). The uranium ions of **4** are pentagonal bipyramidal, featuring a diamond core arrangement of the iodide ligands with *trans*-imido groups and two THF molecules. The U−N distances of 1.879(6) to 1.880(5) Å are typical for *trans*-bis(imido) U(VI)

https://doi.org/10.1021/acs.organomet.4c00449
Organometallics 2025, 44, 289−299

complexes.[39] The U−I distances for the terminal iodides (3.0767(7) to 3.1320(9) Å) are slightly shorter than that of the bridging iodides (3.1770(5) to 3.1920(5) Å).[39] The driving force for the formation of **4** is likely forming the *trans*-bis imido unit, analogous to uranyl.[39] It is hypothesized that formation of **4** is a side product due to the cyclic free base observed in the crystal structure of **2-diazonine**.

While **2-diazonine**, **4**, and the corresponding cyclic free base could not be separated via solubility, their ratio (1:9:21) in the reaction mixture shown in Scheme 4 was approximated through NMR integration. Compound **2-diazonine** is paramagnetic, resonating from −102 to 115 ppm with singlets at 15.46 and 17.99 ppm assigned to $SiMe_3$ groups. Resonances for the endo- and exo-CH_2 groups of the bridge appear at −23.84 and −22.98 ppm. Complex **4** is diamagnetic, with the CH_2 bridge resonance at 5.51 ppm and large, shifted THF resonances at 1.41, 1.52, and 3.58 ppm. The cyclic free base was a majority of this mixture, with large methyl resonances at 0.38 and 0.49 ppm.

Scheme 4. Formation of 2-Diazonine, 4, and Cyclic Free Base from a Geometrically Restrained Diazine

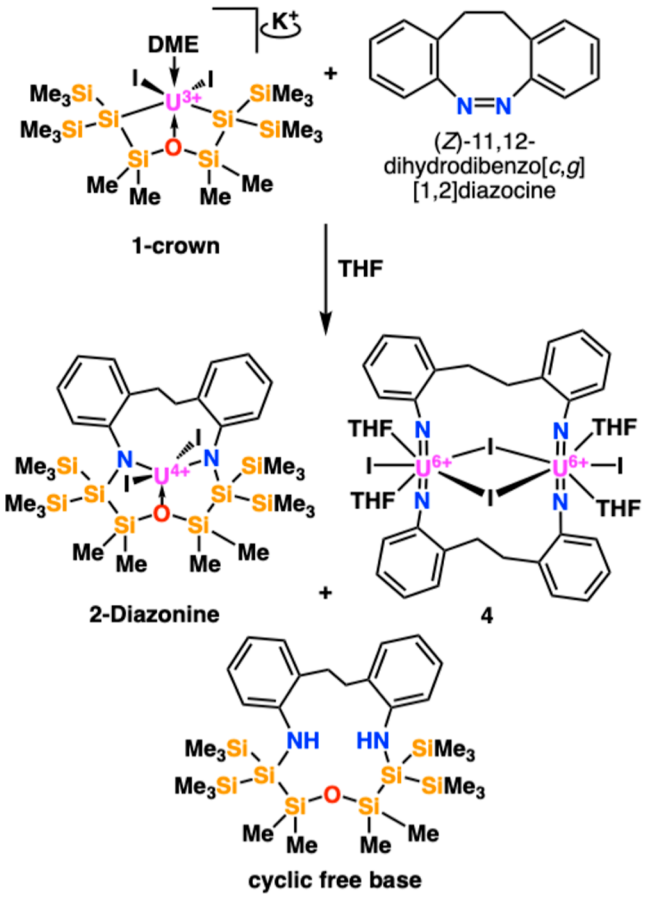

CONCLUSIONS

In summary, treating the silyluranium(III) complex, **1-crown**, with a family of aryl diazenes results in cleavage of the N═N bond, along with insertion into the U−Si bond to generate a series of uranium(IV) products, **2-Ph**, **2-TolPh**, **2-Tol**, **2-F**, **2-OMe**, and **2-Mes**. Increasing the electron-donating character of the aryl diazenes showed some shortening of $U-O_{Si}$ and decrease in N−U−N angle, but very little influence on the the U−N bond. Cyclic voltammetry indicated that the activation of aryl diazenes was favorable with electron-poor N═N bonds, yet was still affected by steric effects imposed by the *ortho*-substitution of the aryl diazene. Mechanistic investigation suggested that solution-symmetric **2-Mes** is formed from an asymmetric U(IV) intermediate, **3-Mes**. The chelating silyl ligand system provides a useful route to stabilizing these low-valent uranium compounds and provides interesting possibilities for activating small molecules. The formation of the family of compounds **2** and **3-Mes** represents a new type of transformation observed with actinide-silyl systems and sheds light on the role of radical recombination to induce silyl migratory insertion and conserve the uranium oxidation state. Overall, this work demonstrates that actinide-silyl species have potentially important roles in organometallic transformations at the bottom of the periodic table.

EXPERIMENTAL SECTION

General Considerations. All air- and moisture-sensitive manipulations were performed using standard Schlenk techniques or using an MBraun inert atmosphere drybox with an atmosphere of purified nitrogen. The MBraun drybox was equipped with a cold well used for freezing samples with liquid nitrogen, dry ice, and acetone baths, as well as two −35 °C freezers for cooling samples and crystallizing compounds. Solvents for sensitive manipulations including THF, toluene, and pentane were dried and deoxygenated using literature procedures with a SecA solvent purification system.[1] 1,2-Dimethoxyethane (DME) was purified by stirring over CaH_2 for at least 2 days before distillation and stored over molecular sieves and sodium. THF-d_8 was purchased from Cambridge Isotope Laboratories (CIL) and stored over sodium in a glovebox freezer. Pyridine-d_5 was purchased from CIL, stirred over CaH_2, distilled, and stored over molecular sieves. Benzene-d_6 (C_6D_6) was purchased from CIL, dried with molecular sieves and sodium, and degassed with three freeze−pump−thaw cycles. $(Me_3Si)_4Si$ was purchased from TCI, and KO^{t}Bu, azobenzene, and 18-crown-6 were purchased from Sigma-Aldrich and used without further purification. Tetrabutylammonium hexafluorophosphate was purchased from Sigma-Aldrich, purified by triple recrystallization, and dried under high vacuum. [K(18-crown-6)][UI_2{(Si(SiMe$_3$)$_2$SiMe$_2$)$_2$O}] (**1-crown**)[2] and aryl diazenes (4-$CF_3C_6H_4N)_2$, (4-$FC_6H_4N)_2$, 4-MeC_6H_4N═NC_6H_5, (4-$MeC_6H_4N)_2$, (4-$OMeC_6H_4N)_2$, (2,6-$Et_2C_6H_3N)_2$, (2,4,6-$Me_3C_6H_2N)_2$, and (2,6-^{i}Pr$_2$C$_6$H$_3$N)$_2$ were synthesized according to literature procedures.[3] (*Z*)-11,12-dihydrodibenzo[*c*,*g*]-[1,2]diazocine was synthesized according to a literature procedure.[4] Gomberg's dimer was synthesized according to a modified literature procedure.[5]

Caution! U-238 is a weak α-emitter with a half-life of $t_{1/2} = 4 \times 10^9$ years. All manipulations were performed in an inert-atmosphere glovebox in a laboratory equipped with proper detection equipment.

^{1}H NMR spectra were recorded on a Varian Inova 300 spectrometer operating at a frequency of 300 MHz, a Bruker AV400 spectrometer operating at a frequency of 400 MHz, or a Bruker DRX-500 or NEO-500 instrument operating at a frequency of 500 MHz. ^{1}H NMR chemical shifts are reported relative to ^{1}H residual chemical shifts of benzene-d_6 (C_6D_6, C_6D_5H = 7.16 ppm), THF-d_8 (1.72 ppm), or pyridine-d_5 (8.74 ppm). For paramagnetic molecules, the ^{1}H NMR data are reported with the chemical shift, followed by the peak-width-

https://doi.org/10.1021/acs.organomet.4c00449
Organometallics 2025, 44, 289−299

at-half-height in Hertz, the integration value, multiplicity, and, where possible, the peak assignment. Multiplicities are assigned as singlet (s), doublet (d), triplet (t), or multiplet (m), and some moieties are abbreviated as trimethylsilyl (Me_3Si or $SiMe_3$). ^{29}Si NMR spectra were recorded on a Bruker AV400, DRX-500 or NEO-500 spectrometer operating at a frequency of 79.49 MHz and sometimes with the ^{29}Si INEPT pulse sequence.[6] A typical ^{29}Si NMR experiment used a 2 s relaxation delay and a 0.5 s acquisition time with a spectral width of 800 ppm. A typical ^{29}Si INEPT NMR experiment used 1s relaxation delay, 0.5 acquisition time, with a spectral width of 800 ppm. ^{29}Si NMR spectra are referenced to an external standard ($(Me_3Si)_4Si$, −9.8 and −135.5 ppm). ^{29}Si NMR signals of **2-Tol**, **2-Ph**, **2 F**, **2-Mes**, **3-Mes**, and **2-diazonine** were unable to be observed due to paramagnetic broadening, and the range searched for ^{29}Si signals were between +600 and −600 ppm. ^{19}F NMR spectra were recorded on a Bruker AV400, DRX-500, or NEO-500 spectrometer operating at a frequency of 376.49 MHz referenced to an internal or external reference of hexafluorobenzene (C_6F_6, −164.9 ppm). Solid-state infrared spectra were recorded using a Thermo Nicolet 6700 spectrophotometer; samples were made by using KBr salt plates or a KBr pellet, and data were notated as weak (w), medium (m), and strong (s). Electronic absorption spectroscopic measurements were recorded at 294 K in sealed 1 cm quartz cuvettes with a Cary 6000i or JASCO V-770 UV/vis−NIR spectrophotometer. Molar absorptivity is reported in units of $\varepsilon = L{\cdot}M^{-1}{\cdot}cm^{-1}$. CHN elemental analyses were performed at Purdue University (West Lafayette, IN). Elemental analyses were attempted but do not meet the "journal standard." We believe that this is due to the high silicon content of these species, as incomplete combustion was noted. We believe this is due to the formation of SiO_2, preventing complete combustion.

Single crystals suitable for X-ray diffraction of **2-F**, **2-Ph**, **2-TolPh**, **2-OMe**, **2-Mes**, **2-MesKI**, and **3-Mes** were coated with poly(isobutylene) oil in the glovebox and quickly transferred to the goniometer head of a Bruker Quest diffractometer with a sealed-tube fine-focus X-ray tube, a single-crystal curved graphite incident beam monochromator, a Photon II area detector, and an Oxford Cryosystems low-temperature device. Examination and data collection were performed with Mo Kα radiation (λ = 0.71073 Å) at 150 K.

Single crystals suitable for X-ray diffraction of **2-Tol** were coated with poly(isobutylene) oil in the glovebox and transferred to the goniometer head of a four-circle Bruker AXS D8 Quest diffractometer with an I-mu-S microsource X-ray tube, Helios multilayer Montel optics, a Photon III C14 charge-integrating and photon-counting pixel array detector, and an Oxford Cryosystems low-temperature device. Examination and data collection were performed with Cu Kα radiation (λ = 1.54178 Å) at 150 K.

Single crystals suitable for X-ray diffraction of **2-diazonine** were coated with poly(isobutylene) oil in the glovebox and transferred to the goniometer head of a Bruker AXS D8 Quest diffractometer with an I-mu-S microsource X-ray tube, laterally graded multilayer (Goebel) optics, a Photon III C14 charge-integrating and photon-counting pixel array detector, and an Oxford Cryosystems low-temperature device. Examination and data collection were performed with Cu Kα radiation (λ = 1.54178 Å) at 150 K.

Electrochemical experiments were carried out using a CHI 620e potentiostat under an inert atmosphere. The electrochemical cell consisted of a glassy carbon working electrode, platinum coil auxiliary electrode, and silver wire reference electrode. Each sample consisted of 0.1 M tetrabutylammonium hexafluorophosphate (NBu_4PF_6) and 3 mM analyte. Potentials were externally and internally referenced versus 3 mM ferrocene (0 V). Cyclic voltametric scans were recorded using 100 mV/s scans, 10 s quiet time, and an appropriate amount of *iR* compensation. Estimated standard deviations for redox couples are ±5 mV.

Synthetic Procedures. *Modified Literature Procedure for the Generation of Gomberg's Dimer ($Ph_3C)_2$.* A 20 mL scintillation vial was charged with a magnetic stir bar, trityl chloride (ca. 1.5 g, 5.4 mmol), and Zn powder (ca. 1 g, 15 mmol). The solids were suspended in 2 mL of dry MeCN and 15 mL of pentane. The mixture was allowed to stir for at least 15 min, sometimes overnight, and the yellow pentane was decanted, filtered through a filter pipet, and the saturated solution allowed to settle in the freezer overnight affording clumps of light yellow crystals. The supernatant was decanted and placed in a trityl chloride/Zn/MeCN vial. This process was repeated several times, affording a combined yield of ca. 0.5 g, 1.1 mmol, and 20% yield of Gomberg's dimer.

General Synthesis of [(THF)U(I)$_2${N(R)Si(SiMe$_3$)$_2$SiMe$_2$}$_2$O] (R = Ph, F, TolPh, Tol, OMe, Diazonine). A typical experiment is described. A 20 mL scintillation vial was charged with a stir bar, **1-crown** (0.025 g, 0.037 mmol), and THF (4 mL), which is cooled to −35 °C in the freezer. Once sufficiently cooled, to the solution was added the aryl diazene (1 equiv, 0.004 g $(4\text{-F-}C_6H_4N)_2$, 0.003 g $(C_6H_5N)_2$, 0.003 g 4-Me-$C_6H_4N{=}NC_6H_5$, 0.004 g $(4\text{-Me}C_6H_4N)_2$, 0.004 g $(4\text{-OMe}C_6H_4N)_2$, 0.005 g $(2,4,6\text{-}Me_3C_6H_2N)_2$, or (*Z*)-11,12-dihydrodibenzo[*c*,*g*][1,2]-diazocine 0.005g (0.037 mmol) as a solid at ambient temperature, immediately producing a color change from blue to brown/orange/yellow. After allowing the solution to stir for 2 h, the volatiles were removed in vacuo and further triturated with pentane (1 × 2 mL) and dried. The yellow/orange solids were washed with pentane (3 × 5 mL), and the brown/yellow solids were eluted with THF. Upon drying the pentane fraction, the solids were identified as **2 F** (0.007 g, 22% yield), **2-Ph** (0.006 g, 28% yield), **2-TolPh** (0.010 g, 43% yield), **2-Tol** (0.006 g, 27% yield), **2-OMe** (0.008g, 34% yield), **2-Mes** (0.006 g, 26% yield*), and **2-diazonine** (0.010 g, 45% yield**). Single crystals suitable for X-ray diffraction were grown from concentrated *n*-pentane or *n*-hexane solutions in a glovebox freezer (−35 °C). ***2-Mes** was isolated on a larger scale in a separate experiment (see synthesis of **3-Mes**). **In this experiment, *trans*-bis-imido uranium(VI) dimer (**4**) was extracted with THF as a brown substance in 0.025 g, 81% yield.

General NMR Scale Experiment of [(THF)U(I)$_2${N(R)Si-(SiMe$_3$)$_2$SiMe$_2$}$_2$O] (R = Ph, F, Ph, Mes). A typical experiment is described. A Teflon-sealed J-Young tube was charged with **1-crown** (0.013 g, 0.010 mmol) and C_6D_6 (0.5 mL) forming a suspension of a light brown solution and a blue solid. To the solution was added a mixture of the aryl diazene (1 equiv, 0.002 g $(4\text{-F-}C_6H_4N)_2$, 0.002 g $(C_6H_5N)_2$, 0.002 g $(4\text{-Me-}C_6H_4N)_2$, 0.003 g $(2,4,6\text{-Me}_3\text{-}C_6H_2N)_2$, 0.010 mmol) and elemental iodine I_2 (0.5 equiv, 0.001 g, 0.004 mmol) at ambient temperature. The tube was shaken, and upon ^{1}H NMR analysis, the compounds in solution were identified.

2-F: ^{1}H NMR (400 MHz, 26 °C, C_6D_6, δ): (ppm) = −27.54 (7.8, 12H, s, $Si(CH_3)_2$), −1.29 (11.7, 66H, s, 18-crown-6), 15.45 (5.0, 36H, s, $Si(CH_3)_3$), 29.12 (8.0, 4H, d, *m*-CH), 78.47

https://doi.org/10.1021/acs.organomet.4c00449
Organometallics 2025, 44, 289−299

(38.7, 4H, s, *o*-CH). ^{19}F NMR (376.46 MHz, 26 °C, C_6D_6, δ): = −83.67 ppm. FTIR (KBr Pellet) ν (cm^{-1}) = 684 (w), 837 (s), 962 (m), 1110 (s), 1246 (m), 1352 (m), 1400 (m), 1507 (m), 2894 (m), 2950 (m), 3134 (m). UV−vis/NIR (THF, 21 °C) wavelength (ε) = 370 (1110), 440 (770), 975 (7), 1080 (10), 1130 (12), 1365 (10), 1380 (13). Elemental analysis: Anal. Calcd for C32H64F2I2N2O2Si8U: C, 30.42%; H, 5.11%; N, 2.22%. Found: C, 46.11%; H, 5.01%, N, 3.48%.

2-Ph: ^{1}H NMR (300 MHz, 23 °C, C_6D_6, δ): (ppm) = −87.4 (31, 8H, s, THF), −30.3 (16, 8H, s, THF), −28.6 (9, 16H, s, $Si(CH_3)_2$), 14.0, (5, 2H, t, *p*-CH), 14.7 (6, 2H, s), 16.5 (5, 2H, s), 16.8 (4, 36H, s, $Si(CH_3)_3$), 25.9 (13, 8H, s, *m*-CH), 68.8 (8H, s, *o*-CH). FTIR (KBr Pellet) ν (cm^{-1}) = 694 (w), 756 (w), 838 (m), 964 (m), 1106 (s), 1249 (m), 1283 (m), 1352 (m), 1400 (w), 1472 (m), 1499 (w), 1578 (w), 1602 (w), 2895 (m). UV−vis/NIR (THF, 21 °C) wavelength (ε) = 1070 (21), 1125 (19), 1385 (16). Elemental analysis: Anal. Calcd for C32H66I2N2O2Si8U: C, 31.31%; H, 5.42%; N, 2.28%. Found: C, 44.50%; H, 9.36%, N, 2.43%.

2-TolPh: ^{1}H NMR (500 MHz, 25 °C, C_6D_6, δ): (ppm) = −85.18 (37.9, 4H, THF), −29.60 (17.8, 4H, s, THF), −28.26 (12.6, 6H, s, tolyl half $Si(CH_3)_2$), −27.66 (12.4, 6H, s, phenyl half $Si(CH_3)_2$), 12.66 (4.3, 3H, s, tolyl CH_3), 16.17 (5.0, 18H, s, phenyl half $Si(CH_3)_3$), 16.61 (4.3, 18H, s, tolyl half $Si(CH_3)_3$), 24.43 (7.3, 2H, s, phenyl *m*-CH), 26.34 (8.9, 2H, d, tolyl *m*-CH), 67.00 (32.3, 2H, s, phenyl *o*-CH), 69.26 (33.2, 2H, s, tolyl *o*-CH). FTIR (KBr Pellet) ν (cm^{-1}) = 621 (w), 694 (w), 837 (m), 964 (m), 1105 (s), 1200 (w), 1248 (m), 1286 (m), 1353 (m), 1398 (w), 1456 (w), 1473 (m), 1598 (w), 2746 (w), 2826 (m), 2893 (m), 2945 (m), 3120 (w). FTIR (KBr Pellet) ν (cm^{-1}) = 621 (w), 694 (w), 837 (s), 964 (s), 1105 (s), 1200 (w), 1248 (m), 1286 (m), 1352 (m), 1398 (w), 1456 (m), 1473 (m), 1598 (w), 2826 (m), 2893 (m), 2946 (m). UV−vis/NIR (THF, 21 °C) wavelength (ε) = 371 (1099), 442 (555), 1013 (8), 1065 (10), 1113 (10), 1385 (16), 1438 (6). Elemental analysis: Anal. Calcd for C33H68I2N2O2Si8U: C, 31.93%; H, 5.52%; N, 2.26%. Found: C, 46.31%; H, 8.14%, N, 4.18%.

2-Tol: ^{1}H NMR (500 MHz, 26 °C, C_6D_6, δ): (ppm) = −84.96 (36.1, 4H, s, THF), −29.49 (17.6, 4H, s, THF), −27.95 (13.5, 12H, s, $SiMe_2$), 15.44 (13.5, 6H, *p*-CH_3), 16.32 (7.2, 36H, s, $SiMe_3$), 25.34 (9.3, 4H, s, *m*-CH), 68.70 (31.2, 4H, s, *o*-CH). FTIR (KBr Pellet) ν (cm^{-1}) = 623 (w), 689 (w), 834 (m), 965 (m), 1100 (s), 1207 (w), 1249 (m), 1285 (w), 1352 (m), 1340 (w), 1467 (w), 1497 (w), 1515 (w), 2564 (w), 2825 (m), 2870 (m), 2894 (m). UV−vis/NIR (THF, 21 °C) wavelength (ε) = 441 (573), 1073 (6), 1117 (6), 1384 (9). Elemental analysis sample decomposed (attempted 3x).

2-OMe: ^{1}H NMR (300 MHz, 23 °C, C_6D_6, δ): (ppm) = −88.5 (8, 2H, s, THF), −30.5 (7, 4H, s, THF), −29.0 (5, 12H, s, $Si(CH_3)_2$), 8.0 (3, 6H, s, *p*-OCH_3), 16.8 (3, 36H, s, $Si(CH_3)_3$), 25.6 (7, 4H, *m*-CH), 72.3 (15, 4H, *o*-CH). ^{29}Si NMR (79.49 MHz, 26 °C, C_6D_6, δ): (ppm) = −91.2 (*Si*Me_3), 143.0 (N*Si*), 172.1 (*Si*Me_2). ^{29}Si INEPT NMR (79.49 MHz, 26 °C, C_6D_6, δ): (ppm) = −91.2 (*Si*Me_3), 172.0 (*Si*Me_2). FTIR (KBr salt plate, pentane): ν (cm^{-1}) = 622 (w), 688 (m), 787 (m), 835 (s), 1035 (m), 1104 (w), 1179 (w), 1244 (s), 1362 (w), 1398 (w), 1441 (w), 1465 (w), 1507 (s), 1599 (w), 2831 (w), 2894 (m), 2950 (m), 3397 (w). UV−vis/NIR (THF, 21 °C) wavelength (ε) = 355 (1934), 369 (1674), 433 (662), 818 (15), 969 (11), 1070 (14), 1125 (15), 1363 (15), 1385 (23). Elemental analysis: Anal. Calcd for C34H70I2N2O4Si8U: C, 31.72%; H, 5.48%; N, 2.18%. Found: C, 28.79%; H, 5.15%, N, 3.48%.

2-Mes: ^{1}H NMR (500 MHz, 26 °C, C_6D_6, δ): (ppm) = −25.96 (21.9, 12H, s, $Si(CH_3)_2$), −3.89 (44.6, 4H, s, *m*-CH), 5.77 (15.5, 6H, s, *o*-CH_3), 11.19 (34.2, 4H, s, *p*−CH_3), 16.81 (19.5, 36H, s, $Si(CH_3)_3$). FTIR (KBr Pellet) ν (cm^{-1}) = 502 (w), 601 (w), 623 (m), 693 (m), 785 (m), 834 (s), 963 (m), 1036 (m), 1110 (m), 1203 (m), 1246 (m), 1287 (m), 1351 (m), 1399 (m), 14,734 (m), 1496 (m), 1583 (m), 1599 (m), 2893 (m), 2950 (m). UV−vis/NIR (THF, 21 °C) wavelength (ε) = 367 (1975), 411 (1702), 835 (25), 957 (16), 1112 (32), 1318 (8), 1400 (25).

2-diazonine: ^{1}H NMR (400 MHz, 26 °C, C_6D_6, δ): (ppm) = −101.99 (45, 1H, s, CH), −97.82 (20, 1H, s, CH), −45.20 (50, 1H, s, CH), −22.98 (8, 2H, s, endo CH_2), −21.70 (7, 2H, s, exo CH_2), −17.27 (137, 12H, s, $Si(CH_3)_2$), −9.80 (4, 2H, s, CH), 15.46 (8, 6H, s, CH_3), 17.99 (6, 6H, s, CH_3), 27.52 (348, 36H, s, $Si(CH_3)_3$), 31.73 (13, 1H, s, CH), 81.46 (22, 1H, s, CH), 114.72 (115, 1H, s, CH).

4: ^{1}H NMR (400 MHz, 26 °C, C_6D_6, δ): (ppm) = 1.41−1.52 (20, 16H, m, THF CH_2), 3.58 (18, 16H, s, THF CH_2), 5.51 (38, 8H, br s, CH_2), 7.08−8.45 (m, 12 x CH).

Synthesis of Compound 3-Mes. Synthesis A: Separate THF solutions of **1-crown** (0.022 g, 0.016 mmol, 6 mL THF) and a mixture (4 mL THF) of MesN = NMes (0.004 g, 0.015 mmol) and Gomberg's dimer (0.004 g, 0.008 mmol) were cooled to −35 °C in a glovebox freezer. The mixture of MesN═NMes and Gomberg's dimer were added to **1-crown** dropwise over 2 min. The solution was allowed to stir while warming to ambient temperature for 3 h. Volatiles were removed in vacuo, and the solids were washed with pentane to remove Ph_3CI, and **3-Mes** was extracted with Et_2O.

Synthesis B: Separate solutions of **1-crown** (0.100 g, 0.073 mmol, 10 mL THF) and MesN═NMes (0.018 g, 0.068 mmol, 1.07 equiv, 4 mL THF) were cooled to −35 °C in a glovebox freezer. To **1-crown**, the MesN═NMes solution was added dropwise over 2 min. The solution was allowed to stir while warming up to ambient temperature for 3 h, revealing a dark orange solution. ^{1}H NMR of the crude solution indicated a 49:51 ratio of **2-Mes:3-Mes** by integration. Volatiles were removed in vacuo, and the powder was washed with pentane through a medium-porosity frit (5 × 5 mL). The yellow pentane extract solution was set aside, and the solvent evaporated to obtain a first batch of **2-Mes**. The orange solids in the filter cake on the frit were dissolved in minimal Et_2O and left in the glovebox freezer overnight, precipitating yellow crystals that were combined with the first batch of **2-Mes** (**2-Mes**, 0.035 g, 36% combined isolated yield). The orange Et_2O solution was decanted and further layered with pentane in a 1:1 ratio. Upon allowing the biphasic solution to settle in the freezer for 3 days, single large red−orange crystals were isolated and analyzed by X-ray diffraction revealing **3-Mes**. ^{1}H NMR of the orange powder upon drying revealed clean **3-Mes** in 25% isolated yield (0.026 g).

3-Mes ^{1}H NMR (400 MHz, 26 °C, C_6D_6, δ): (ppm) = −100.33 (115, 3H, s, CH_3), −17.21 (40, 9H, s, $Si(CH_3)_3$) −16.06 (10, 9H, s, $Si(CH_3)_3$), −14.30 (11, 9H, s, $Si(CH_3)_3$), −14.04 (10, 1H, s, CH), 12.21 (54, 3H, s, CH_3), 2.40 (18, 24H, s, 18-crown-6), 13.64 (14, 1H, s, CH), 15.53 (15, 1H, s, CH), 20.90 (15, 1H, s, CH), 27.44 (24, 3H, s, CH_3), 27.99 (35, 3H, s, CH_3), 30.17 (12, 3H, s, CH_3), 37.45 (61, 6H, s, $Si(CH_3)_2$), 45.22 (13, 2H, *m*−CH), 50.10 (14, 3H, s, CH_3). FTIR (KBr salt plate, C_6D_6) ν (cm^{-1}) = 678 (m), 812 (s), 836

https://doi.org/10.1021/acs.organomet.4c00449
Organometallics 2025, 44, 289−299

(s), 963 (m), 1011 (w), 1110 (m), 1246 (m), 1274 (m), 1301 (m), 1330 (m), 1351 (m), 1471 (m), 1617 (w), 2361 (w), 2893 (m), 2947 (m), 3235 (w). UV−vis/NIR (THF, 21 °C) wavelength (ε): 335 (2732), 568 (202), 723 (100), 841 (42), 890 (26), 1040 (17), 1095 (16), 1195 (19), 1222 (13).

■ ASSOCIATED CONTENT

Supporting Information

The Supporting Information is available free of charge at https://pubs.acs.org/doi/10.1021/acs.organomet.4c00449.

Spectroscopic data (PDF)

Accession Codes

Deposition Numbers 2325803−2325806, 2325808, 2325810, 2325812, 2345044, and 2349482−2349483 contain the supplementary crystallographic data for this paper. These data can be obtained free of charge via the joint Cambridge Crystallographic Data Centre (CCDC) and Fachinformationszentrum Karlsruhe Access Structures service.

■ AUTHOR INFORMATION

Corresponding Author

Suzanne C. Bart − *H. C. Brown Laboratory, James Tarpo Jr. and Margaret Tarpo Department of Chemistry, Purdue University, West Lafayette, Indiana 47907, United States;* orcid.org/0000-0002-8918-9051; Email: sbart@purdue.edu

Authors

Nathan J. Lin − *H. C. Brown Laboratory, James Tarpo Jr. and Margaret Tarpo Department of Chemistry, Purdue University, West Lafayette, Indiana 47907, United States*

Kelly L. Gullett − *H. C. Brown Laboratory, James Tarpo Jr. and Margaret Tarpo Department of Chemistry, Purdue University, West Lafayette, Indiana 47907, United States*

Ushindi K. Muna − *H. C. Brown Laboratory, James Tarpo Jr. and Margaret Tarpo Department of Chemistry, Purdue University, West Lafayette, Indiana 47907, United States*

Ryan Galloway − *H. C. Brown Laboratory, James Tarpo Jr. and Margaret Tarpo Department of Chemistry, Purdue University, West Lafayette, Indiana 47907, United States; Department of Chemistry and Biochemistry, Presbyterian College, Clinton, South Carolina 29325, United States*

Matthias Zeller − *H. C. Brown Laboratory, James Tarpo Jr. and Margaret Tarpo Department of Chemistry, Purdue University, West Lafayette, Indiana 47907, United States;* orcid.org/0000-0002-3305-852X

Complete contact information is available at: https://pubs.acs.org/10.1021/acs.organomet.4c00449

Author Contributions

The manuscript was written through contributions of all authors. All authors have given approval to the final version of the manuscript.

Notes

The authors declare no competing financial interest.

■ ACKNOWLEDGMENTS

The authors acknowledge Dr. John Harwood for assistance with ^{29}Si NMR spectroscopy. The authors acknowledge a grant from the National Science Foundation (CHE-2247452, grant to S.C.B.). The authors acknowledge Chris Rybak from Purdue University for providing clean samples of (*Z*)-11,12-dihydrodibenzo[*c*,*g*][1,2]diazocine.

■ REFERENCES

(1) Braunstein, P.; Knorr, M. Reactivity of the Metal-Silicon Bond in Organometallic Chemistry. *J. Organomet. Chem.* **1995**, *500* (1), 21−38.

(2) Marciniec, B.; Maciejewski, H.; Pietraszuk, C.; Pawluć, P. *Advances in Silicon Science−Hydrosilylation: A Comprehensive Review on Recent Advances*; Springer, 2009.

(3) Troegel, D.; Stohrer, J. Recent Advances and Actual Challenges in Late Transition Metal Catalyzed Hydrosilylation of Olefins from an Industrial Point of View. *Coord. Chem. Rev.* **2011**, *255* (13), 1440−1459.

(4) Fry, J. L.; Rahaim, Jr., R. J.; Maleczka, Jr., R. E. *Encyclopedia of Reagents for Organic Synthesis*; John Wiley & Sons, Ltd, 2007.

(5) Zaranek, M.; Pawluc, P. Markovnikov Hydrosilylation of Alkenes: How an Oddity Becomes the Goal. *ACS Catal.* **2018**, *8* (10), 9865−9876.

(6) Aylett, B. J. Some Aspects of Silicon-Transition Metal Chemistry. *Adv. Inorg. Chem.* **1982**, *25*, 1−133.

(7) Bald, J. F.; MacDiarmid, A. G. Synthesis of Silylammonium and Silylphosphosnium Compounds by the Reaction of Amines and Phosphines with Silylcobalt Tetracarbonyls. *J. Organomet. Chem.* **1970**, *22* (2), C22−C24.

(8) Corriu, R. J. P.; Moreau, J. J. E.; Pataud-Sat, M. Silyliron Carbonyl Complexes in Organic Synthesis: Selective Conversion of Nitriles into N,N-Bis(Silyl) Enamines. *Organometallics* **1985**, *4* (4), 623−629.

(9) Arnold, J.; Tilley, T. D. Insertion of Organic Carbonyls into the Tantalum-Silicon Bond of (η^5-C_5Me_5)Cl_3TaSiMe_3. Preparation and Characterization of the α-Silylalkoxides (η^5-C_5Me_5)-Cl_3TaOCRR'SiMe_3. *J. Am. Chem. Soc.* **1987**, *109* (11), 3318−3322.

(10) Ignatov, S. K.; Khalimon, A. Y.; Rees, N. H.; Razuvaev, A. G.; Mountford, P.; Nikonov, G. I. β-Agostic Silylamido and Silyl-Hydrido Compounds of Molybdenum and Tungsten. *Inorg. Chem.* **2009**, *48* (20), 9605−9622.

(11) Khalimon, A. Y.; Ignatov, S. K.; Simionescu, R.; Kuzmina, L. G.; Howard, J. A. K.; Nikonov, G. I. An Unexpected Mechanism of Hydrosilylation by a Silyl Hydride Complex of Molybdenum. *Inorg. Chem.* **2012**, *51* (2), 754−756.

(12) Nikonov, G. I.; Mountford, P.; Dubberley, S. R. Tantalizing Chemistry of the Half-Sandwich Silylhydride Complexes of Niobium: Identification of Likely Intermediates on the Way to Agostic Complexes. *Inorg. Chem.* **2003**, *42* (2), 258−260.

(13) Réant, B. L. L.; Berryman, V. E. J.; Seed, J. A.; Basford, A. R.; Formanuik, A.; Wooles, A. J.; Kaltsoyannis, N.; Liddle, S. T.; Mills, D. P. Polarised Covalent Thorium(IV)− and Uranium(IV)−Silicon Bonds. *Chem. Commun.* **2020**, *56* (83), 12620−12623.

(14) Gransbury, G. K.; Réant, B. L. L.; Wooles, A. J.; Emerson-King, J.; Chilton, N. F.; Liddle, S. T.; Mills, D. P. Electronic Structure Comparisons of Isostructural Early D- and f-Block Metal(III) Bis(Cyclopentadienyl) Silanide Complexes. *Chem. Sci.* **2023**, *14* (3), 621−634.

(15) Réant, B. L. L.; De Alwis Jayasinghe, D.; Wooles, A. J.; Liddle, S. T.; Mills, D. P. Comparison of Group 4 and Thorium M(IV) Substituted Cyclopentadienyl Silanide Complexes. *Dalton Trans.* **2023**, *52* (22), 7635−7645.

(16) King, W. A.; Marks, T. J. Metal-Silicon Bonding Energetics in Organo-Group 4 and Organo—f-Element Complexes. Implications for Bonding and Reactivity. *Inorg. Chim. Acta* **1995**, *229* (1−2), 343−354.

(17) Nolan, S. P.; Porchia, M.; Marks, T. J. Organo-f-Element Thermochemistry. Actinide-Group 14 Element and Actinide-Transition-Element Bond Disruption Enthalpies and Stoichiometric/Catalytic Chemical Implications Thereof in Heterobimetallic Tris(Cyclopentadienyl)Uranium(IV) Compounds. *Organometallics* **1991**, *10* (5), 1450−1457.

(18) Réant, B. L. L.; Liddle, S. T.; Mills, D. P. F-Element Silicon and Heavy Tetrel Chemistry. *Chem. Sci.* **2020**, *11* (40), 10871−10886.
(19) Diaconescu, P. L.; Odom, A. L.; Agapie, T.; Cummins, C. C. Uranium−Group 14 Element Single Bonds: Isolation and Characterization of a Uranium(IV) Silyl Species. *Organometallics* **2001**, *20* (24), 4993−4995.
(20) Porchia, M.; Brianese, N.; Casellato, U.; Ossola, F.; Rossetto, G.; Zanella, P.; Graziani, R. Tri(η-Cyclopentadienyl)Uranium(IV) Silyl and Siloxide Compounds. Crystal Structure of $[U(\eta^5\text{-}C_5H_5)_3(OSiPh_3)]$. Insertion of Lsocyanide into a Uranium−Silicon Bond. *J. Chem. Soc., Dalton Trans.* **1989**, *0* (4), 677−681.
(21) Brackbill, I. J.; Douair, I.; Lussier, D.; Boreen, M.; Maron, L.; Arnold, J. Synthesis and Structure of Uranium−Silylene Complexes. *Chem. - Eur. J.* **2020**, *26* (11), 2360−2364.
(22) Lin, N.; Zeller, M.; Bart, S. C. Solution and Solid-State Characterization of Rare Silyluranium(III) Complexes. *Chem. Commun.* **2024**, *60*, 3954.
(23) Zitz, R.; Hlina, J.; Aghazadeh Meshgi, M.; Krenn, H.; Marschner, C.; Szilvási, T.; Baumgartner, J. Using Functionalized Silyl Ligands To Suppress Solvent Coordination to Silyl Lanthanide(II) Complexes. *Inorg. Chem.* **2017**, *56* (9), 5328−5341.
(24) Pöcheim, A.; Marschner, C.; Baumgartner, J. Rare-Earth−Silyl Ate-Complexes Opening a Door to Selective Manipulations. *Inorg. Chem.* **2021**, *60* (11), 8218−8226.
(25) Lewis, A. J.; Williams, U. J.; Carroll, P. J.; Schelter, E. J. Tetrakis(Bis(Trimethylsilyl)Amido)Uranium(IV): Synthesis and Reactivity. *Inorg. Chem.* **2013**, *52* (13), 7326−7328.
(26) McCullough, L. G.; Turner, H. W.; Andersen, R. A.; Zalkin, A.; Templeton, D. H. Preparation and Crystal Structure of the 1,2-Dimethoxyethane Complex of Bis[Bis(Trimethylsilyl)Amido]-Dichlorouranium(IV). *Inorg. Chem.* **1981**, *20* (9), 2869−2871.
(27) Berthet, J.-C.; Thuéry, P.; Ephritikhine, M. New Efficient Synthesis of $[UI_4(MeCN)_4]$. X-Ray Crystal Structures of $[UI_2(MeCN)_7][UI_6]$, $[UI_4(Py)_3]$, and $[U(Dmf)_9]I_4$. *Inorg. Chem.* **2005**, *44* (4), 1142−1146.
(28) Carmichael, C. D.; Jones, N. A.; Arnold, P. L. Low-Valent Uranium Iodides: Straightforward Solution Syntheses of UI3 and UI4 Etherates. *Inorg. Chem.* **2008**, *47* (19), 8577−8579.
(29) Réant, B. L. L.; Wooles, A. J.; Liddle, S. T.; Mills, D. P. Synthesis and Characterization of Yttrium Methanediide Silanide Complexes. *Inorg. Chem.* **2023**, *62* (1), 137−146.
(30) Windorff, C. J.; Evans, W. J. ^{29}Si NMR Spectra of Silicon-Containing Uranium Complexes. *Organometallics* **2014**, *33* (14), 3786−3791.
(31) Arnold, P. L.; Jones, G. M.; Odoh, S. O.; Schreckenbach, G.; Magnani, N.; Love, J. B. Strongly Coupled Binuclear Uranium−Oxo Complexes from Uranyl Oxo Rearrangement and Reductive Silylation. *Nat. Chem.* **2012**, *4* (3), 221−227.
(32) Liddle, S. T. The Renaissance of Non-Aqueous Uranium Chemistry. *Angew. Chem., Int. Ed.* **2015**, *54* (30), 8604−8641.
(33) Monreal, M. J.; Thomson, R. K.; Cantat, T.; Travia, N. E.; Scott, B. L.; Kiplinger, J. L. UI_4(1,4-Dioxane)$_2$, $[UCl_4$(1,4-Dioxane)$]_2$, and UI_3(1,4-Dioxane)$_{1.5}$: Stable and Versatile Starting Materials for Low- and High-Valent Uranium Chemistry. *Organometallics* **2011**, *30* (7), 2031−2038.
(34) Perales, D.; Ford, S. A.; Salpage, S. R.; Collins, T. S.; Zeller, M.; Hanson, K.; Bart, S. C. Conversion of Trivalent Uranium Anilido to Tetravalent Uranium Imido Species via Oxidative Deprotonation. *Inorg. Chem.* **2020**, *59* (17), 11910−11914.
(35) Perales, D.; Lin, N. J.; Bronstetter, M. R.; Ford, S. A.; Zeller, M.; Bart, S. C. Conversion of Uranium(III) Anilido Complexes to Uranium(IV) Imido Complexes via Hydrogen Atom Transfer. *Organometallics* **2022**, *41* (5), 606−616.
(36) Andersen, R. A. Tris((Hexamethyldisilyl)Amido)Uranium(III): Preparation and Coordination Chemistry. *Inorg. Chem.* **1979**, *18* (6), 1507−1509.
(37) Goodwin, C. A. P.; Tuna, F.; McInnes, E. J. L.; Liddle, S. T.; McMaster, J.; Vitorica-Yrezabal, I. J.; Mills, D. P. $[U^{III}\{N(SiMe_2tBu)_2\}_3]$: A Structurally Authenticated Trigonal Planar Actinide Complex. *Chem. - Eur. J.* **2014**, *20* (45), 14579−14583.
(38) Goodwin, C. A. P.; Mills, D. P. Silylamides.: Towards a Half-Century of Stabilising Remarkable f-Element Chemistry. In *Organometallic Chemistry: Vol. 41*; Fairlamb, I., Lynam, J. M., Patmore, N. J., Elliott, P., Eds.; The Royal Society of Chemistry, 2017; Vol. *41*, pp 123−156.
(39) Hayton, T. W.; Boncella, J. M.; Scott, B. L.; Palmer, P. D.; Batista, E. R.; Hay, P. J. Synthesis of Imido Analogs of the Uranyl Ion. *Science* **2005**, *310* (5756), 1941−1943.

https://doi.org/10.1021/acs.organomet.4c00449
Organometallics 2025, 44, 289−299